Received: 12 October 2023 | Revised: 4 January 2024 | Accepted: 10 January 2024

DOI: 10.1111/jpi.12941

ORIGINAL ARTICLE

Journal of Pineal Research — Molecular, Biological, Physiological and Clinical Aspects of Melatonin | WILEY

Binding and unbinding of potent melatonin receptor ligands: Mechanistic simulations and experimental evidence

Annalida Bedini[1] | **Gian Marco Elisi**[2] | **Fabiola Fanini**[1] | **Michele Retini**[1] | **Laura Scalvini**[2] | **Silvia Pasquini**[3] | **Chiara Contri**[4] | **Katia Varani**[4] | **Gilberto Spadoni**[1] | **Marco Mor**[2] | **Fabrizio Vincenzi**[4] | **Silvia Rivara**[2]

[1]Dipartimento di Scienze Biomolecolari, Università degli Studi di Urbino Carlo Bo, Urbino, Italy

[2]Dipartimento di Scienze degli Alimenti e del Farmaco, Università degli Studi di Parma, Parma, Italy

[3]Dipartimento di Scienze Chimiche, Farmaceutiche ed Agrarie, Università degli Studi di Ferrara, Ferrara, Italy

[4]Dipartimento di Medicina Traslazionale, Università degli Studi di Ferrara, Ferrara, Italy

Correspondence

Silvia Rivara, Dipartimento di Scienze degli Alimenti e del Farmaco, Università degli Studi di Parma, Parco Area delle Scienze 27/A, Parma I-43124, Italy.
Email: silvia.rivara@unipr.it

Fabrizio Vincenzi, Dipartimento di Medicina Traslazionale, Università degli Studi di Ferrara, Via Luigi Borsari 46, Ferrara I-44121, Italy.
Email: fabrizio.vincenzi@unife.it

Funding information

Italian Ministry for University and Research (MUR), Grant/Award Number: PRIN 2017, 20175SA5JJ project; MUR funded by the European Union, Grant/Award Numbers: NextGenerationEU, CUPD93C22000930002, 4.2.1.3

Abstract

The labeled ligand commonly employed in competition binding studies for melatonin receptor ligands, 2-[^{125}I]iodomelatonin, showed slow dissociation with different half-lives at the two receptor subtypes. This may affect the operational measures of affinity constants, which at short incubation times could not be obtained in equilibrium conditions, and structure–activity relationships, as the K_i values of tested ligands could depend on either interaction at the binding site or the dissociation path. To address these issues, the kinetic and saturation binding parameters of 2-[^{125}I]iodomelatonin as well as the competition constants for a series of representative ligands were measured at a short (2 h) and a long (20 h) incubation time. Concurrently, we simulated by molecular modeling the dissociation path of 2-iodomelatonin from MT_1 and MT_2 receptors and investigated the role of interactions at the binding site on the stereoselectivity observed for the enantiomers of the subtype-selective ligand UCM1014. We found that equilibrium conditions for 2-[^{125}I]iodomelatonin binding can be reached only with long incubation times, particularly for the MT_2 receptor subtype, for which a time of 20 h approximates this condition. On the other hand, measured K_i values for a set of ligands including agonists, antagonists, nonselective, and subtype-selective compounds were not significantly affected by the length of incubation, suggesting that structure–activity relationships based on data collected at shorter time reflect different interactions at the binding site. Molecular modeling simulations evidenced that the slower dissociation of 2-iodomelatonin from the MT_2 receptor can be related to the restricted mobility

Annalida Bedini and Gian Marco Elisi should be considered first joint authors.

Fabrizio Vincenzi and Silvia Rivara should be considered joint senior authors.

(MNESYS), FSE-REACT-EU, PONRI 2014-2020, CUPH31B21009610007-research contract, 63-G-19602-1

of a gatekeeper tyrosine along a lipophilic path from the binding site to the membrane bilayer. The enantiomers of the potent, MT_2-selective agonist UCM1014 were separately synthesized and tested. Molecular dynamics simulations of the receptor–ligand complexes provided an explanation for their stereoselectivity as due to the preference shown by the eutomer at the binding site for the most abundant axial conformation adopted by the ligand in solution. These results suggest that, despite the slow-binding kinetics occurring for the labeled ligand, affinity measures at shorter incubation times give robust results consistent with known structure–activity relationships and with interactions taken at the receptor binding site.

KEYWORDS

2-iodomelatonin, binding kinetics, free-energy simulations, melatonin receptors, stereoselectivity, UCM1014, unbinding

1 | INTRODUCTION

Determination of binding affinity of melatonin receptor ligands mostly relies on the use of the MT_1/MT_2 nonselective radioligand 2-[^{125}I]iodomelatonin in displacement binding assays.[1,2] 2-Iodomelatonin is characterized by high binding affinity at both subtypes and high specific activity.[3] Commonly, membrane preparations from recombinant cells expressing human MT_1 or MT_2 receptors are incubated with 2-[^{125}I]iodomelatonin and the ligand of interest for a period of 1–3 h, assuming that equilibrium conditions are established at those times.[4–7] On the other hand, investigation of the binding kinetics of 2-[^{125}I]iodomelatonin revealed a slow dissociation rate. While the dissociation half-life of 2-[^{125}I]iodomelatonin at MT_1 receptors expressed in CHO cell membranes was estimated to be ~50 min at 37°C,[8,9] a residence time at the MT_2 receptor could not be calculated due to the incomplete dissociation observed in the experiment time (2 h).[9]

Slow dissociation of the labeled ligand could delay the equilibrium condition in competition studies, and this raises the doubt that incubation times commonly applied to MT_1/MT_2 binding affinity determinations for new ligands might be too short to provide reliable and robust inhibition constants. Additionally, different dissociation kinetics from receptor subtypes could affect experimental measures of ligand selectivity. In fact, there are cases where selective occupation of a receptor can be achieved in vivo by drugs that dissociate more quickly from a different subtype.[10] For example, the bronchodilator tiotropium is characterized by very slow dissociation from the muscarinic M_3 receptor, which results in kinetic selectivity over M_1 and M_2 subtypes.[11,12] With these premises, binding data for melatonin receptors and the corresponding structure–activity relationships, which are critical for advancing newly designed compounds to in vivo studies, should be re-evaluated assessing the dependence of the "apparent" binding constants from time-related aspects of binding protocols.

From a mechanistic point of view, slow binding also raises the doubt if the pharmacophoric features of a specific class of ligands depend more on the association/dissociation path or on the interactions taken at the binding site. This information is determinant for the choice of the predictive models to apply in the design of new ligands[13] and in the exploitation of structure–activity relationships. In fact, while investigations on structure–activity relationships for G protein-coupled receptor ligands and their design have been generally based on binding-interaction models, recently different modeling protocols have been developed to reproduce the unbinding process of slow-binding drugs.[14,15] These two aspects of ligand-binding kinetics, significant for the design and optimization of novel melatonin receptor ligands, at the moment are both overlooked. A way to solve this problem in a mechanistic framework is combining consistent binding data for reference and potent ligands with modeling simulations.

In this context, we set up and performed a series of experiments and modeling simulations to assess the impact of time-dependent binding between MT_1 and MT_2 receptors and representative ligands on structure–activity relationships investigated by molecular modeling. To this aim, we initially assessed the kinetic and saturation binding parameters of the labeled ligand 2-[^{125}I]iodomelatonin on membrane preparations obtained from CHO cells stably expressing the MT_1 or MT_2 receptors and

compared the k_{off} for the two receptor subtypes with unbinding simulations based on a lipophilic pathway hypothesis.[16] We then measured apparent K_i at different incubation times in competition experiments for a small set of potent ligands including melatonin, the non-selective agonist 2-phenylmelatonin[17] and antagonist luzindole,[18] the MT_2-selective antagonist UCM800,[5] and the potent and selective MT_2 agonist UCM1014[19] (Figure 1). As our provisional results suggested that apparent binding parameters obtained with standardized protocols were sufficiently robust and related more to interactions at the binding site than to the unbinding path, we tested this working hypothesis by simulating binding interactions for two enantiomers of the potent ligand UCM1014, which had been previously characterized as a racemic mixture only.[19] We then synthesized the two enantiomers separately with known stereochemistry and validated the stereoselectivity predictions made by molecular modeling simulations.

2 | MATERIALS AND METHODS

2.1 | Chemistry

(+)-(*R*)-UCM1014 and (−)-(*S*)-UCM1014 were obtained by optical resolution of a precursor compound which was reacted with a resolving agent and then submitted to chromatographic separation of the resulting diastereoisomers. After removal of the chiral auxiliary, each stereoisomer was converted into the final UCM1014 enantiomer through synthetic steps that do not involve the stereogenic center. The absolute configuration of (+)-(*R*)-UCM1014 and (−)-(*S*)-UCM1014 was deduced from that of precursor stereoisomers, by comparison of ^{1}H NMR spectra with those of enantiopure structural analogs. The detailed description of the synthetic strategy, characterization of newly synthesized compounds, and absolute configuration attribution is reported in Supporting Information S1: Section 1.1.

2.2 | Pharmacology

2.2.1 | Binding experiments

Binding experiments were performed by using membranes obtained from CHO cells transfected with hMT_1 or hMT_2 receptors and 2-[^{125}I]iodomelatonin (specific activity 2200 Ci/mmol, Perkin Elmer). Incubations were performed at 37°C in binding buffer consisting of 50 mM Tris-HCl, pH 7.4, 5 mM $MgCl_2$. At the end of the incubation time, bound and free radioactivity were separated in a Brandel cell harvester (Brandel Instruments) by filtering the assay mixture through Whatman GF/B glass fiber filters. The filter-bound radioactivity was counted in a 2810 TR liquid scintillation counter (Perkin Elmer). More details can be found in Supporting Information S1: Sections 1.2.1–1.2.4.

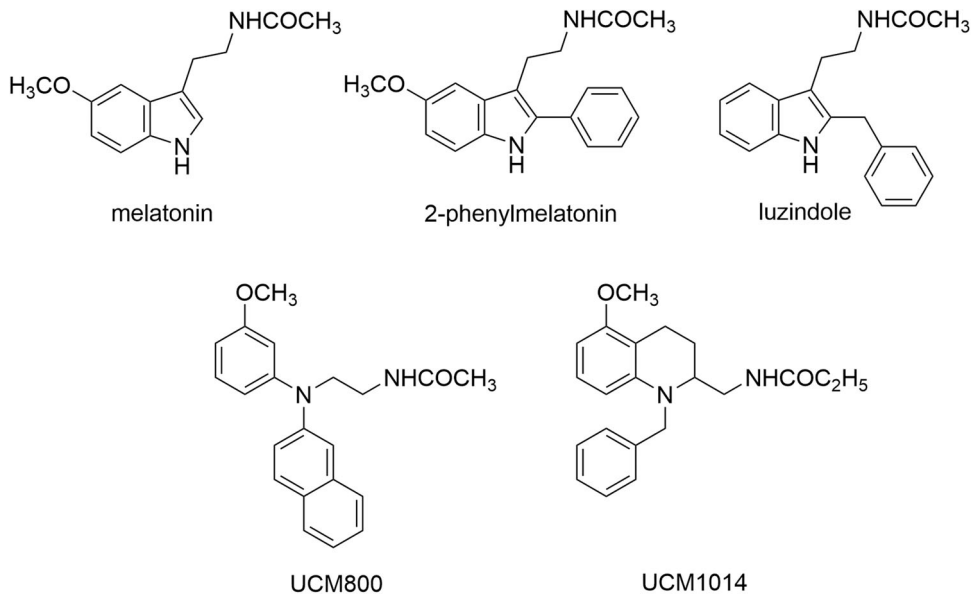

FIGURE 1 Melatonin receptor ligands evaluated in competition experiments toward 2-[^{125}I]iodomelatonin with 2 and 20 h incubation time: the natural ligand melatonin, the agonist 2-phenylmelatonin, the antagonist luzindole, the MT_2-selective antagonist UCM800 and the MT_2-selective agonist UCM1014.

2.2.2 | 3′,5′-Cyclic adenosine monophosphate (cAMP) assays

cAMP levels were quantified using the AlphaScreen cAMP Detection Kit (Perkin Elmer), following the manufacturer's instructions. Additional details are provided in the Supporting Information S1: Section 1.2.5.

2.3 | Molecular modeling

2.3.1 | Molecular dynamics (MD) simulations

The crystal structures of 2-iodomelatonin (PDB id 6ME4[16]) and 2-phenylmelatonin (PDB code 6ME6[20]) in complex with MT_1 and MT_2 receptors in their inactive form were prepared for molecular simulations. The phenyl ring of 2-phenylmelatonin was replaced with an iodine atom (Supporting Information S1: Section 1.3.1). The complexes of MT_1 and MT_2 receptor with UCM1014 enantiomers were obtained through docking calculations (Supporting Information S1: Section 1.3.2). Details about the systems preparation are provided in Supporting Information S1: Section 1.3.3.

MD simulations were performed using Gromacs 2019.2.[21] Biased simulations, in which a bias potential is deposited along certain degrees of freedom of the system, called collective variables (CVs), were conducted by patching the MD code with Plumed 2.5.4.[22] Long-range electrostatics were computed with the Particle Mesh Ewald summation,[23] while short-range and Lennard–Jones interactions were computed within a 10 Å cut-off. The LINCS algorithm[24] was adopted to restrain bond lengths of hydrogens bound to heavy atoms to their equilibrium values, to set an integration timestep of 2 fs. MD simulations were performed in canonical ensemble at a temperature of 298 K enforced through the Nosé–Hoover thermostat[25,26] with a coupling constant of 0.5 ps.

2.3.2 | Umbrella sampling (US) simulations

US simulations[27] were performed using a CV specifically designed to simulate the unbinding of 2-iodomelatonin from the MT_1 and MT_2 receptors through the lipophilic channel between transmembrane (TM) helices IV and V (for additional details see Supporting Information S1: Section 1.3.4 and Figure S5). For each US simulation, input coordinates were obtained through initial steered MD simulations followed by a relaxation stage (Supporting Information S1: Section 1.3.5). Afterward, a bias potential in the form of a harmonic restraint was kept for 40 ns at each unitary value of the explored range of the unbinding CV ($-1 \leq CV_{unb} \leq 15$Å), with a spring constant of 5 kcal mol^{-1} Å^{-2}. Free-energy profiles were reconstructed applying the weighted histogram analysis method (WHAM) algorithm,[28] on an averaged time-series of converged potential of mean force (PMF) profiles (Supporting Information S1: Section S2.2.1 and Figures S7–S9). An alternative unbinding route toward the extracellular region was also simulated for the MT_2 receptor (see Supporting Information S1: Section 1.3.6).

2.3.3 | Well-tempered metadynamics simulation

Well-tempered metadynamics[29] was employed to evaluate the conformational space of (*R*)-UCM1014 bound at the MT_1 and MT_2 receptor, after 1.0 μs of unrestrained MD was performed to equilibrate the system. A biasing potential in the form of Gaussian hills was deposited on the phase space defined by the ligand torsion angle τ_1 (defined in Figure 6). The Gaussian width was fixed to 0.035 rad (~2°), the initial Gaussian height was set to 0.15 kcal mol^{-1}. A slow deposition frequency of 50 ps^{-1} was implemented. Hills height was rescaled over time by adopting a bias factor of 10. Simulations lasted for 500 ns and convergence was checked by monitoring the diffusiveness of the CV and the difference between free-energy minima over time (Supporting Information S1: Section 2.2.2 and Figure S10).[30,31]

3 | RESULTS

3.1 | Determination of 2-iodomelatonin binding parameters

Kinetic parameters of 2-[^{125}I]iodomelatonin binding were measured on membrane preparations obtained from CHO cells stably transfected with human MT_1 or MT_2 receptors (Table 1). One crucial finding from kinetic

TABLE 1 Kinetic binding parameters of 2-[^{125}I]iodomelatonin for human MT_1 and MT_2 receptors.[a]

	k_{on} (M^{-1} min^{-1})	k_{off} (min^{-1})	Dissociation $t_{1/2}$ (min)
MT_1	$1.2 \pm 0.1 \times 10^8$	0.0028 ± 0.0002	248 ± 20
MT_2	$3.7 \pm 0.3 \times 10^7$	0.000639 ± 0.000054	1085 ± 98

[a]Kinetic parameters were measured on membranes from CHO cells expressing either human MT_1 or MT_2 receptors. Results are given as mean ± SEM ($n = 3$).

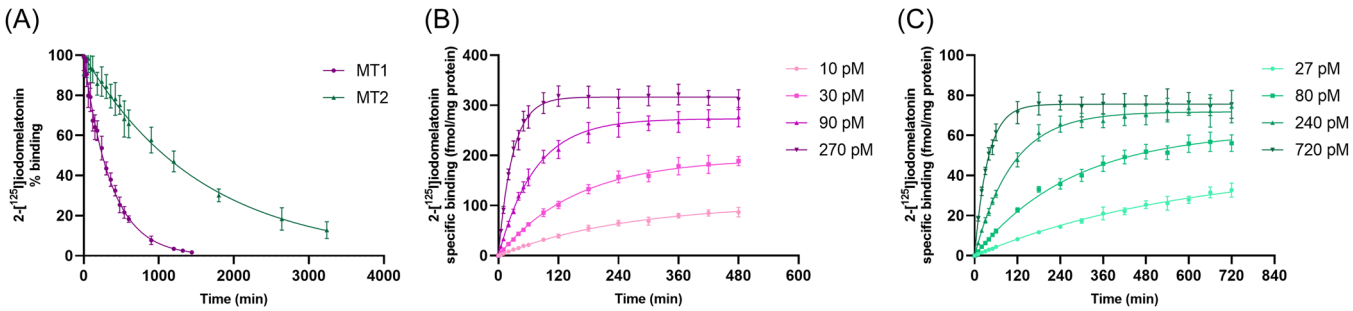

FIGURE 2 Dissociation curves (A) of 2-[^{125}I]iodomelatonin for MT_1 (purple) and MT_2 (green) receptors. Association curves of 2-[^{125}I]iodomelatonin for MT_1 (B) and MT_2 (C) receptors at four different radioligand concentrations as indicated. Data are the mean ± SEM of three independent experiments.

binding studies is that 2-[^{125}I]iodomelatonin exhibits slow dissociation, especially from the MT_2 receptor (Figure 2A). In particular, we observed a dissociation half-life ($t_{1/2}$) of approximately 4 h for the MT_1 receptor and a significantly longer half-life of 18 h for the MT_2 receptor. Association kinetic experiments highlighted faster association of the ligand at the MT_1 receptor than at the MT_2 receptor, consistently with previous observations.[9] Based on the association curves obtained at radioligand concentrations commonly employed in competition experiments (30 pM for MT_1 and 80 pM for MT_2), the calculated values of the k_{obs} were 0.0036 and 0.0064 min, respectively (Figure 2B,C). This translates to association half-lives of 108 min for MT_1 and 193 min for MT_2 at those specific concentrations.

To evaluate the time-dependence of the "apparent" binding constants (K_D) that result from experiments at fixed times, saturation binding curves were obtained at two different incubation times, that is, 2 h, consistent with those usually adopted in binding affinity assays, and 20 h, which should guarantee the equilibrium condition at least for the MT_1 receptor. Given that achieving equilibrium requires five times the dissociation $t_{1/2}$,[32] conducting saturation binding experiments at MT_2 receptors would necessitate significantly longer incubation times (approximately 90 h). However, experiments at longer times were not performed because protein degradation could in such cases affect experimental results. In spite of the significant difference of incubation times, K_D values obtained fitting saturation binding curves (Table 2) showed similar values at short and long incubation times, with minimal decreases at longer experimental times. After Scatchard linearization, saturation isotherms showed a monophasic profile at both receptors, indicating the presence of a single class of binding sites (Supporting Information S1: Figure S6). The maximum number of binding sites is also conserved at longer times, being lower for the MT_2 receptor than for the MT_1 one.

TABLE 2 Saturation binding parameters of 2-[^{125}I]iodomelatonin for human MT_1 and MT_2 receptors.[a]

Receptor	Incubation time (h)	K_D (pM)	Bmax (fmol mg^{-1} protein)
MT_1	2	26 ± 2	342 ± 26
MT_1	20	19 ± 2	329 ± 31
MT_2	2	78 ± 5	76 ± 7
MT_2	20	65 ± 4	74 ± 6

[a]Values obtained from CHO cells expressing either human MT_1 or MT_2 receptors. Results are given as mean ± SEM ($n = 3$).

3.2 | Time dependency of ligand binding affinity at MT_1 and MT_2 receptors

Once established that a 20-h incubation period ensures equilibrium of the radioligand concentrations used in competition binding experiments, while a 2-h incubation does not, even if the differences in apparent K_D are small, the time dependency of ligand binding affinity was further investigated in competition experiments using a set of compounds characterized by different intrinsic activity and selectivity at melatonin receptors. These include melatonin, the nonselective agonist 2-phenylmelatonin,[17] the nonselective antagonist luzindole,[18] and two non-indolic MT_2-selective ligands, the agonist UCM1014[19] and the antagonist UCM800[5] (Figure 1). As the potent ligand UCM1014 had been previously characterized only as a racemic mixture,[19] to compare experimental binding data and the outputs of molecular simulations (vide infra), we separately synthesized the two enantiomers with known configuration (see Supporting Information for synthesis and characterization). For all compounds, incubation time affected only weakly the binding affinity constants measured at both receptors, as can be seen from K_i values reported in Table 3 for experiments performed at 2 and 20 h of incubation. The highest difference in binding affinity at

TABLE 3 Affinity of melatonergic ligands for human MT_1 and MT_2 receptors expressed in CHO cells at different incubation times (2 or 20 h).[a]

Compound	MT_1 K_i (nM) 2 h	MT_1 K_i (nM) 20 h	MT_2 K_i (nM) 2 h	MT_2 K_i (nM) 20 h
Melatonin	0.240 ± 0.016	0.114 ± 0.008	0.326 ± 0.022	0.159 ± 0.013
2-Phenylmelatonin	0.036 ± 0.002	0.029 ± 0.002	0.040 ± 0.003	0.033 ± 0.003
Luzindole	367 ± 24	401 ± 28	14.2 ± 1.1	17.4 ± 1.3
UCM800	102 ± 8	176 ± 15	0.510 ± 0.038	0.732 ± 0.058
UCM1014	18.3 ± 1.6	4.64 ± 0.39	0.058 ± 0.004	0.033 ± 0.002
(*R*)-UCM1014	7.23 ± 0.61	1.48 ± 0.12	0.045 ± 0.004	0.028 ± 0.002
(*S*)-UCM1014	91 ± 8	74 ± 6	2.10 ± 0.17	6.12 ± 0.45

[a]K_i values were calculated from IC_{50} values, obtained from competition curves by the method of Cheng and Prusoff.[33] Results are given as mean ± SEM ($n = 3$).

TABLE 4 Potency of melatonergic ligands for human MT_1 and MT_2 receptors in cAMP assay.[a]

Compound	MT_1 IC_{50} (nM)	MT_1 (Pharmacological behavior)	MT_2 IC_{50} (nM)	MT_2 (Pharmacological behavior)
Melatonin	0.277 ± 0.024	Full agonist	0.975 ± 0.087	Full agonist
UCM800[b]	332 ± 26	Antagonist	1.75 ± 0.11	Antagonist
UCM1014	31 ± 2	Full agonist	0.436 ± 0.035	Full agonist
(*R*)-UCM1014	12.4 ± 1.1	Full agonist	0.245 ± 0.019	Full agonist
(*S*)-UCM1014	290 ± 23	Full agonist	9.32 ± 0.77	Full agonist

Abbreviation: cAMP, 3′,5′-Cyclic adenosine monophosphate.

[a]IC_{50} is the concentration of compound that reduces by 50% the production of cAMP induced by 1 μM of forskolin.

[b]The antagonist UCM800 was tested in the presence of 0.3 nM melatonin for the MT_1 receptor and 1 nM melatonin for the MT_2 receptor, along with 1 μM forskolin. Results are given as mean ± SEM ($n = 3$).

the two timepoints was detected for (*R*)-UCM1014, which showed about fivefold increased MT_1 affinity at 20 h, with no significant difference in subtype selectivity. Despite our kinetic data suggest that the optimal condition for competition experiments with melatonin receptors, particularly MT_2, requires longer incubation times to ensure that equilibrium is reached, the apparent K_i values obtained at different times show that for a representative set of ligands, including both agonists and antagonists, structure–activity relationships are conserved when binding data collected at shorter times are considered.

The melatonergic ligands were evaluated for their intrinsic activity with the cAMP assay (Table 4), confirming the agonist or antagonist behavior previously obtained in the guanosine 5′-O-(3-thiotriphosphate) test. These assays provide consistent evidence on the ability of the tested ligands to recruit G protein. Nevertheless, a different behavior in other signaling systems (e.g., β-arrestin) cannot be ruled out, potentially leading to agonist bias,[34] as observed for other melatonergic ligands.[35] The agonist/antagonist profile of ligands should also be confirmed in physiological settings, as receptor overexpression in recombinant cells could lead to deviations in signaling outcomes that may not accurately reflect responses in native conditions.[36] This is particularly relevant for melatonergic ligands as the activation of the various signaling pathways is highly context-specific, and could be different at the level of cell type or tissue under consideration.[37]

3.3 | Unbinding simulations of 2-iodomelatonin from MT_1 and MT_2 receptors

To provide a mechanistic explanation of the different dissociation half-life observed for 2-iodomelatonin at the two receptor subtypes, we performed US simulations on receptor–ligand complexes in which the ligand was forced to progressively leave the receptor binding site and move into the membrane bilayer passing through a

TM channel, following a path that had been previously identified within crystallographic structures,[16] described by modeling simulations[38] and supported by mutagenesis data.[20,39] An unbinding collective variable (CV_{unb}) joining the ligand-binding site and the membrane bilayer was defined and the conformational space of the complex was sampled by a set of 40 ns-long MD simulations (see Supporting Information S1: Section 1.3.4 for details) with the center of mass of 2-iodomelatonin constrained at fixed values of the CV_{unb} ($-1 \le CV_{unb} \le 15$ Å). At the highest value of CV_{unb} the ligand has passed beyond TM helices IV and V and is in contact with the lipid bilayer. The PMF profiles for unbinding along CV_{unb}, calculated by WHAM[28] from the simulations of the two ligand–receptor complexes, evidence that 2-iodomelatonin has to overcome a dissociation barrier of ~16.0 and ~20 kcal mol^{-1} at the MT_1 and MT_2 receptors, respectively (Figure 3). These energy barriers are consistent with the longer dissociation half-life measured at the MT_2 receptor, albeit they underestimate the experimental ones (24.2 kcal mol^{-1} for MT_1 receptor and 25.1 kcal mol^{-1} for MT_2 receptor, calculated from k_{off} values) and overestimate the energy difference between the two receptor subtypes, which may be attributed to model approximations and/or incomplete exploration of the conformational space.

The free-energy profile within the binding site ($-1 \le CV_{unb} \le 2$ Å) is almost identical for the two receptors, suggesting similar interactions involved in the stabilization of the ligand–receptor complexes. A difference in the two PMF curves is observed in the interval $4 \le CV_{unb} \le 8$ Å, where the local minimum at CV_{unb} = 5–6 Å corresponds to a configuration in which the indole ring of 2-iodomelatonin is positioned between helices IV and V of the MT_1 receptor (Figure 4). Another difference is observed at CV_{unb} = 13–14 Å, where interactions with residues on the surface of the TM portion (e.g., Ala158$^{4.56}$, Asn162$^{4.60}$, Ballesteros–Weinstein numbering[40] in superscripts) cause a small minimum for the MT_1 receptor. The main molecular determinant of the

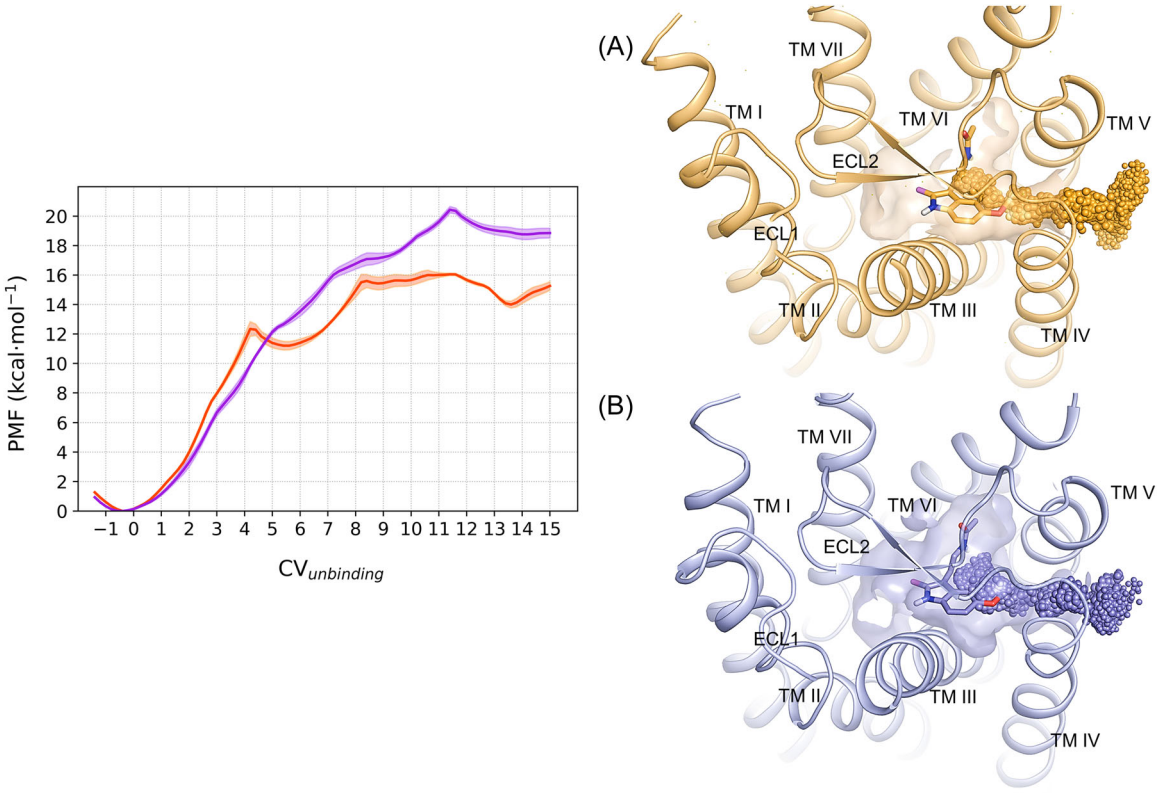

FIGURE 3 Left panel: potential of mean force (PMF) profiles calculated for 2-iodomelatonin unbinding from the MT_1 (red line) and MT_2 receptor (purple line) across the lipophilic channel between transmembrane (TM) helices IV and V. Shaded areas represent standard deviation of the free energy. CV_{unb} = 0 Å corresponds to 2-iodomelatonin bound to the orthosteric binding site; at CV_{unb} = 15 Å the ligand has crossed the lipophilic channel and is in the membrane bilayer. Right panel: the unbinding pathway of 2-iodomelatonin is represented through the position of the center of mass of the ligand registered every 100 ps during umbrella sampling simulations at the MT_1 (A, orange) and MT_2 (B, purple) receptors. In the simulations, 2-iodomelatonin exits through the lipophilic channel between TM helices IV and V, depicted as a surface around the ligand and buried within the TM bundle by ECL2.

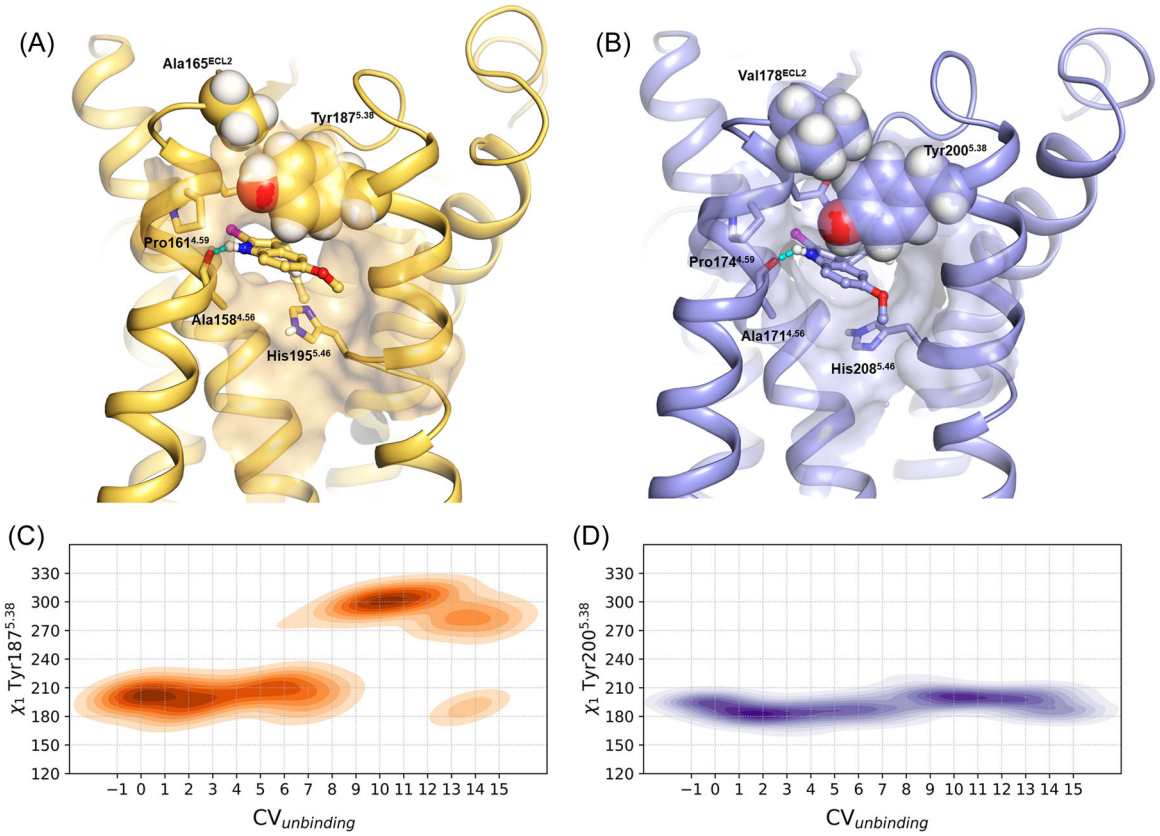

FIGURE 4 Representative snapshots of 2-iodomelatonin (ball and sticks) unbinding, showing the indole ring inside the lipophilic channel between transmembrane (TM) helices IV and V (corresponding to $CV_{unb} = 6$ Å) at the MT_1 (A, orange) and MT_2 (B, purple) receptors. Hydrogen bonds between the ligand and Ala158/161$^{4.56}$ are shown in cyan. Tyr187/200$^{5.38}$ and Ala165/Val178^{ECL2} are shown with Van der Waals representation. Lower panels: density estimation plots showing χ_1 dihedral angle of Tyr187/200$^{5.38}$ in umbrella sampling simulations at the MT_1 (C) and MT_2 (D) receptors ($\chi_1 = 180°$, closed conformation; $\chi_1 = 300°$, open conformation). Tyr200$^{5.38}$ in the MT_2 receptor maintains a closed conformation, while Tyr187$^{5.38}$ in the MT_1 receptor changes conformation to an open arrangement during ligand egress from the binding site.

different PMF curves is Tyr187/200$^{5.38}$, located at the entrance of the TM channel (Figure 4). During unbinding from the MT_1 receptor, the side chain of Tyr187$^{5.38}$ is initially in a "closed" conformation ($\chi_1 = 180°$) pointing toward TM IV and opens upon 2-iodomelatonin passage toward the lipid bilayer. Once ligand exit is completed, the side chain returns to the closed state. The behavior of Tyr200$^{5.38}$ at the MT_2 receptor is different, as it maintains the closed state during ligand path. As a consequence, His208$^{5.46}$ enters the binding site at $4 \leq CV_{unb} \leq 8$Å, favoring ligand egress from the receptor (Supporting Information S1: Figure S11). Thus, the higher energetic barrier for the unbinding of 2-iodomelatonin from the MT_2 receptor seems to be related more to a structural difference in the receptor architecture, that is, the preference for a closed conformation of the gatekeeper tyrosine, than to specific interactions between the ligand and different amino acids encountered during the path toward the lipid bilayer.

Analysis of crystal structures of melatonin receptor complexes allowed to hypothesize an alternative access route to the ligand binding site from the solvent-exposed extracellular region.[20] This secondary route was also investigated by means of the same computational protocol applied for the lipophilic pathway. 2-Iodomelatonin was forced to leave the binding site of the MT_2 receptor and reach the extracellular environment. The PMF calculated from US simulations evidenced a significantly higher free-energy barrier compared to the lipophilic pathway (Figure 5), supporting a preference for the latter one. The conformation of Tyr294$^{7.39}$ seen in crystal structures obstructs the ligand path. The peak in the PMF profile occurring around $CV_{unb} = 8$–9 Å corresponds to a change of Tyr294$^{7.39}$ χ_1 dihedral angle allowing for ligand egress. Notably, mutation of Tyr294$^{7.39}$ to alanine caused a 20-fold reduction of [^{3}H]-melatonin residence time.[20]

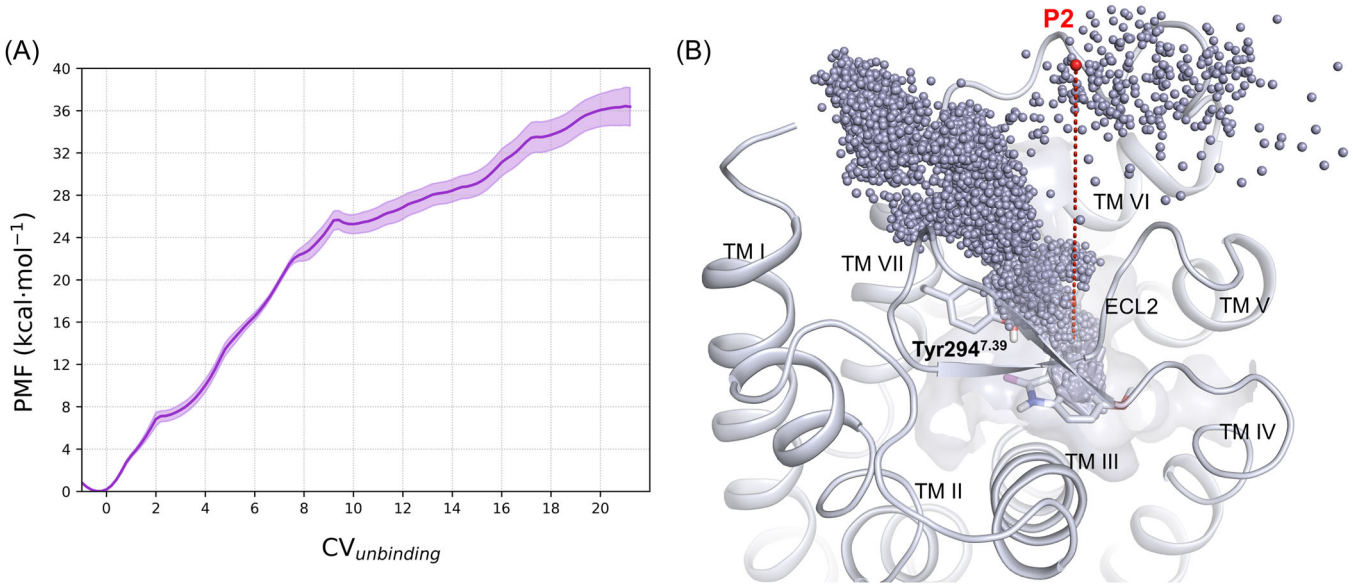

FIGURE 5 (A) Potential of mean force (PMF) profile calculated for 2-iodomelatonin unbinding from the MT_2 receptor (purple line) following an extracellular unbinding route. Shaded areas represent standard deviation of the free energy. $CV_{unb} = 0$ Å corresponds to 2-iodomelatonin bound to the orthosteric binding site. At $CV_{unb} = 20$ Å the ligand is solvated in the extracellular environment. (B) The unbinding pathway of 2-iodomelatonin along the extracellular route is represented through the position of the center of mass, which is registered every 100 ps during umbrella sampling simulations. The red line represents the axis defining the collective variable.

3.4 | Molecular modeling at the binding site: Stereoselectivity of UCM1014 enantiomers

The hypothesis that unbinding kinetics from the two receptor subtypes depends on receptor, more than ligand, structure involves that operational binding affinities for different ligands (and thus structure–activity relationships) should reflect interactions at the binding site, more than the path covered by the ligand. To test this hypothesis, we evaluated the ability of molecular models reproducing binding complexes to predict the stereoselectivity for the two newly synthesized enantiomers of the potent, MT_2-selective agonist UCM1014. As shown in Table 3, the (*R*)-enantiomer of UCM1014 resulted the eutomer, with about 160-fold selectivity for the MT_2 receptor after 2 h of incubation. Molecular docking in the MT_2 receptor showed a different preferred conformation within the binding site, with the amide side chain assuming an axial arrangement in (*R*)-UCM1014 (corresponding to the torsion angle $\tau_1 = -68°$, as defined in Figure 6C) and an equatorial one in (*S*)-UCM1014 ($\tau_1 = 60°$) (Figure 6). Both enantiomers interacted with $Gln194^{ECL2}$, similarly to what had been observed for the amide side chain of crystallized agonists. The docking poses are characterized by similar values of the scoring function (GScore = −10.7 and −10.8 kcal mol^{-1}, respectively) which do not explain the different binding affinities measured for the two enantiomers. Therefore, 1 μs-long MD simulations were run to investigate the stability of the (*R*)- and (*S*)-UCM1014-receptor complexes. While the (*R*)-enantiomer maintained a stable H-bond with $Gln194^{ECL2}$, the amide side chain of the (*S*)-enantiomer showed higher mobility, being bound to $Gln194^{ECL2}$ for the first 300 ns, or interacting with it through water molecules (300–650 ns), then moving to $Asn268^{6.52}$ (650–750 ns) before returning to $Gln194^{ECL2}$ until the end of the simulation (Supporting Information S1: Figures S12 and S13). Interactions of the methoxy group with $Asn175^{4.60}$ were occasional for both enantiomers. Although this suggests a better stabilization for the (*R*)-enantiomer, the change of H-bonding partner for the distomer is not sufficient to definitely explain its lower affinity, because replacement of $Gln194^{ECL2}$ with $Asn268^{6.52}$ as the binding counterpart is consistent with the functional redundance described for the two residues. In fact, mutation of either residue had only minor effects on the affinity of reference ligands and on receptor activation, while mutation of both residues significantly reduced receptor activity.[20]

During MD simulations, the docked conformation of the tetrahydroquinoline scaffold was conserved, that is, with axial amide side chain for the (*R*)-enantiomer and equatorial for the (*S*)-enantiomer. NMR data of the desmethoxy analog of UCM1014 in solution had shown that the conformations with the tetrahydroquinoline ring having axial side chain are strongly favored.[19] This raises the hypothesis that, while both enantiomers could bind the MT_2 receptor in one of the two ring conformations, binding in the unfavoured conformation with equatorial side chain, would pay an energetic cost that reduces

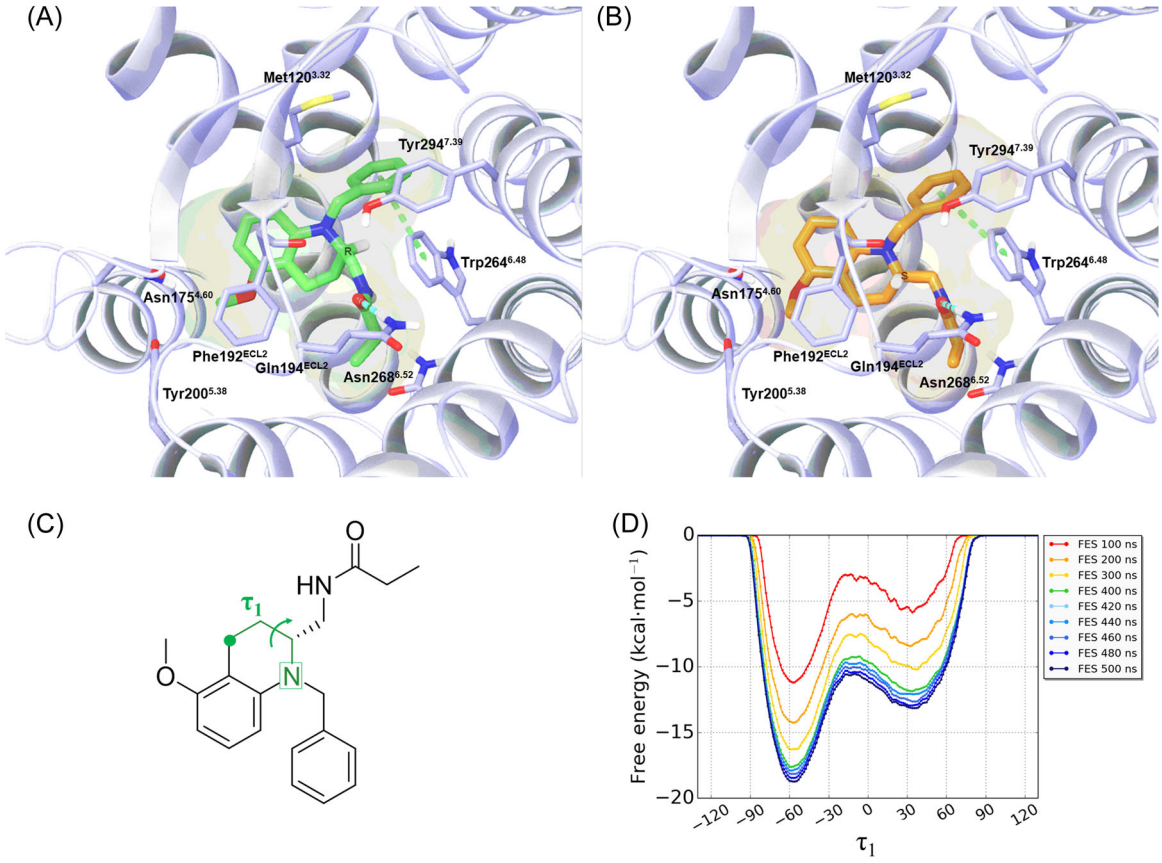

FIGURE 6 Docking poses obtained for (*R*)-UCM1014 (A, green carbons) and (*S*)-UCM1014 (B, orange carbons) in the MT_2 receptor after energy minimization of the complexes. Hydrogen bond between the ligand amide side chain and $Gln194^{ECL2}$ is shown with cyan dotted line; π–π interaction between the benzyl group and $Trp264^{6.48}$ is shown with green dotted line. (C) Definition of τ_1 torsion angle, N-C2-C3-C4, with green atoms and bonds. (D) Time-evolution of the free-energy surface of τ_1 dihedral angle obtained via well-tempered metadynamics simulation of (*R*)-UCM1014 and showing the axial-equatorial equilibrium of the amide side chain inside the MT_2 receptor binding site (axial arrangement of the side chain: $\tau_1 = -60°$; equatorial arrangement: $\tau_1 = 40°$).

ligand affinity. The distomer, (*S*)-enantiomer, in its conformation with axial side chain, cannot interact with $Gln194^{ECL2}$. On the other hand, we verified that the axial arrangement of the (*R*)-enantiomer is preferred within the MT_2 binding site by exploring the ligand conformational space through a metadynamics simulation of the ligand-receptor complex. The τ_1 dihedral angle of (*R*)-UCM1014 was selected as CV and forced to explore the conformations of the tetrahydroquinoline ring, passing from the axial to the equatorial arrangement of the amide side chain. The axial arrangement ($\tau_1 = -60°$) appeared highly favored (Figure 6D), even if also the equatorial one ($\tau_1 = 40°$) could undertake interactions with $Gln194^{ECL2}$. Therefore, the higher binding affinity of (*R*)-UCM1014 can be ascribed to the favorable accommodation of the most populated conformations with axial side chain within the binding site. Moreover, docking simulations (Supporting Information S1: Figure S14) revealed that also in the MT_1 receptor the (*R*)-enantiomer takes optimal interaction in its axial conformation, while for the (*S*)-enantiomer the best pose taking the usual contacts with binding-site residues has an equatorial conformation. Additionally, metadynamics simulations of the conformational equilibria of the (*R*)-enantiomer within the MT_1 binding site confirmed the axial arrangement of the amide side chain as the preferred one (Supporting Information S1: Figure S15). Although both potency and stereoselectivity for this subtype were lower, a receptor model based on a crystal structure can provide an output in accordance with experimental data also in this case.

4 | DISCUSSION

In the past decades, the design of novel melatonergic ligands with improved potency, subtype selectivity or tailored intrinsic activity was mostly based on structure–activity relationships inferred from binding affinity data collected at short incubation times.[41,42]

Despite the availability of tritiated melatonin and the recent development of other radiolabelled ligands,[43,44] most binding affinity data were obtained from displacement assays with 2-iodomelatonin as the labeled ligand. On the other hand, the slow 2-[^{125}I]iodomelatonin binding kinetics raises a question on the impact of the experimental incubation time on binding affinity data (K_i) obtained in competition studies. In fact, the usual incubation period of 1–3 h for competition experiments does not guarantee to reach an equilibrium condition for the radioligand binding/unbinding processes and might affect the binding affinity values obtained for new ligands.[45] In principle, this issue could have a strong impact on drug design because it challenges the assumption that affinity measured at equilibrium for different ligands (and receptors) only depends on interactions taken by the ligand in the solvent and at the binding site. In this scenario, fitting parameters of binding curves should be taken at longer incubation times, ensuring equilibrium conditions. Otherwise, kinetic binding constants should be derived and molecular models should simulate binding/unbinding paths to account for structure–activity relationships.

Given this premise, we determined the binding kinetics of 2-[^{125}I]iodomelatonin in membranes from CHO cells expressing the MT_1 or MT_2 receptors and its binding affinity in saturation experiments at a short (2 h) and a long (20 h) incubation time. Our data showed slow dissociation rates, particularly at the MT_2 receptor for which a dissociation half-life of about 18 h was calculated, consistently with what had been previously observed.[9] A list of the kinetic parameters available for 2-[^{125}I]iodomelatonin and [^{3}H]melatonin at MT_1 and MT_2 receptors is reported in Table 5.

In such a case, the optimal condition for binding experiments occurs at longer times, that more closely approximate the equilibrium conditions of the radioligand: when employing 2-[^{125}I]iodomelatonin concentrations close to its K_D in competition experiments, 20 h incubation time ensures satisfactory equilibrium for both MT_1 and MT_2 receptors. While in principle notable differences in affinity data may emerge for compounds characterized by even slower association and dissociation kinetics compared to 2-iodomelatonin, our data showed that incubation time had very limited effect on the binding affinity parameters in competition experiments performed for a set of ligands comprising agonist and antagonist compounds. These results allow to define the domain of application for molecular modeling simulations to investigate ligand–receptor interactions and for the development of predictive structure–activity relationships. In particular, while kinetic properties like the different dissociation half-lives of 2-iodomelatonin at the two receptor subtypes require models accounting for the unbinding path, our data support the hypothesis that differences in apparent binding constants for similar ligands can be explained by models only reproducing interactions at the binding site.

While a free-energy profile for the unbinding of 2-iodomelatonin from its binding site through a lipophilic route had been calculated by US on a path-CV for MT_1 receptor only,[38] a mechanistic explanation for the longer dissociation half-life of 2-iodomelatonin at the MT_2 receptor was searched comparing two new US simulations with a distance-based CV (see Supporting Information), requiring less computational resources than the previous method.

The simulations, in which 2-iodomelatonin was forced to leave the receptor through a lipophilic pathway across the TM helices, showed a similar behavior of the ligand within the MT_1 and MT_2 binding sites and free energy content ($-1 \leq CV_{unb} \leq 4$), suggesting that the different unbinding rates are not due to a different stabilization of the ligand-receptor complexes. A major difference in the MT_1/MT_2 unbinding free energy profile was observed at the ligand crossing of TM helices ($4 \leq CV_{unb} \leq 8$). Even if the three-dimensional structures of both receptors show an opening between TM helices IV and V, the different mobility of Tyr200$^{5.38}$, located at the entrance of the TM channel, hampers ligand unbinding from the MT_2 receptor. Tyr200$^{5.38}$ maintains a "closed" conformation and undertakes interactions with neighboring residues on TM helix IV (i.e., Ala171$^{4.56}$ and Asn175$^{4.60}$). This conformational preference, as already observed in metadynamics simulations on the residue side chain,[38] is likely due to the proximity of the bulky Val178^{ECL2} limiting the conformational freedom of Tyr200$^{5.38}$. The smaller Ala165^{ECL2} in the MT_1 receptor, corresponding to the MT_2 Val178^{ECL2}, allows for an easier MT_1 Tyr187$^{5.38}$ opening, facilitating 2-iodomelatonin egress from the receptor. Thus, the simulations presented here allowed to confirm that the observed differences in dissociation half-lives should be attributed to the different conformational flexibility of the two receptors, which, in turn, can be explained by the different protein environments of the gating tyrosine. Mutagenesis studies support the involvement of Tyr187/200$^{5.38}$ in affecting ligand unbinding, as replacement of Tyr with Ala produces a greater reduction of melatonin residence time at the MT_2 receptor, leading to similar k_{off} values at the two receptor subtypes.[20] A relevant aspect characterizing 2-iodomelatonin unbinding from the MT_1 receptor is the interaction with residues on the surface of TM helices, responsible for the local minimum observed at CV_{unb} = 13–14 Å. An analogous behavior was observed in a previous study of 2-iodomelatonin unbinding from the MT_1 receptor based on a different enhanced sampling technique.[38] This external contact might represent a recognition event

TABLE 5 Kinetic parameters of 2-[^{125}I]iodomelatonin and [^{3}H]melatonin reported in the literature for the MT_1 and MT_2 receptors.

Ligand	Temp. (°C)	Rec.	Association $t_{1/2}$ (min)	Dissociation $t_{1/2}$ (min)	k_{on} (M^{-1} min^{-1})	k_{off} (min^{-1})	Ref.
2-[^{125}I]IMLT	25	hMT_1	48.6 ± 6.7[a]	48.6 ± 6.7	5.75×10^8	0.01446	[9]
2-[^{125}I]IMLT	25	hMT_2	79.9 ± 9.9[a]	-[b]	3.36×10^8	-	[9]
2-[^{125}I]IMLT	37	hMT_1	20.5 ± 4.2	48.6 ± 12.5	1.32×10^9	0.0153	[9]
2-[^{125}I]IMLT	37	hMT_2	36.4 ± 4.1	-[c]	7.38×10^8	-	[9]
2-[^{125}I]IMLT	37	hMT_1	-	-	$1.10 \pm 0.11 \times 10^9$	0.0134 ± 0.0023	[8]
2-[^{125}I]IMLT	37	hMT_1	108[d]	248 ± 20	$1.2 \pm 0.1 \times 10^8$	0.0028 ± 0.0002	[f]
2-[^{125}I]IMLT	37	hMT_2	193[e]	1085 ± 98	$3.7 \pm 0.3 \times 10^7$	0.000639 ± 0.000054	[f]
[^{3}H]MLT	37	hMT_1	3.0 ± 0.6[g]	33.6 ± 2.9	3.66×10^8	0.02124	[9]
[^{3}H]MLT	37	hMT_2	2.6 ± 0.7[g] 16.6 ± 5.7[g]	69.3 ± 8.2	4.42×10^8 6.78×10^7	0.00852	[9]
[^{3}H]MLT	25	hMT_1	-	37 ± 3.3[h]	-	-	[20]
[^{3}H]MLT	37	hMT_2	-	227 ± 10[h]	-	-	[20]

[a]Calculated at a concentration of 2-[^{125}I]iodomelatonin of 25 pM.
[b]No measurable dissociation.
[c]Only partial dissociation.
[d]Calculated at a concentration of 2-[^{125}I]iodomelatonin of 30 pM.
[e]Calculated at a concentration of 2-[^{125}I]iodomelatonin of 80 pM.
[f]This paper.
[g]Calculated at a concentration of [^{3}H]melatonin of 0.6 nM.
[h]Residence time $(k_{off})^{-1}$.

favoring ligand extraction from the membrane and driving the accommodation within the binding site.[46] Additionally, the binding region at the protein–lipid interface might act as an allosteric site to be exploited for the design of compounds with desired properties.[16,47] This might help in devising MT_1 receptor ligands, for which the molecular determinants conferring selectivity versus the MT_2 receptor have been clarified only partially.[41,42] Structure–activity relationship analysis identified bulky lipophilic substituents replacing the methoxy group of melatonin as a structural feature conferring MT_1-selectivity. These substituents are expected to reside close to TM IV and V and could be fine-tuned to favor interactions with the TM gap and protein-lipid interface. This region might also offer accommodation for bitopic compounds that associate melatonergic activity with pharmacological activity at a different target,[48,49] as recently reported for dual-acting compounds combining melatonin receptor agonism and fatty acid amide hydrolase inhibition for enhanced neuroprotection.[50,51]

An important point in the structure–activity relationships at melatonin receptors is the different binding kinetics of [^{3}H]melatonin and 2-[^{125}I]iodomelatonin. While both 2-[^{125}I]iodomelatonin and [^{3}H]melatonin have shorter dissociation half-life at the MT_1 than at the MT_2 receptor, the latter ligand has higher association and dissociation rates at both receptors. Considering the kinetic data reported for these two ligands in the literature, the insertion of a 2-iodine atom on melatonin structure does not modify the ratio of MT_2/MT_1 dissociation half-lives, being approximately two to six times for [^{3}H]melatonin and four times for 2-[^{125}I] iodomelatonin (Table 5). On the other hand, different effects could concur to the slower dissociation of 2-[^{125}I] iodomelatonin, the most likely being of steric nature, as the presence of the bulky iodine could hamper the crossing of the narrow lipophilic channel. Additionally, the interactions taken by the iodine atom with residues of the lipophilic subpocket at the binding site, known to accommodate substituents in position 2 of the indole ring,[16] could delay the unbinding of the ligand. A further explanation for the faster binding kinetics of [^{3}H] melatonin could be based on the existence of binding routes alternative to the lipophilic one.[20] In fact, while our simulations seem to exclude a cytoplasmic unbinding route for 2-iodomelatonin, a smaller and less lipophilic ligand such as melatonin may benefit from an additional route, oriented toward the solvent-exposed extracellular region. Finally, the electronic density and/or polarizability of the iodine atom might favor attractive interactions with residues approached during the unbinding process.

The description of this kind of interactions requires the application of force fields including polarizability terms, which were not considered in the molecular simulations here reported.

Although the rationalization for the slower MT_2 dissociation rate of 2-iodomelatonin required expensive unbinding simulations, the similar binding affinities observed at short and long incubation times suggest that observed structure–activity relationships could be more related to interactions undertaken within the binding site than to binding/unbinding kinetics. This would allow to investigate structure–activity relationships by computational models based on receptor–ligand complexes at the bound state, thus avoiding the expensive simulations of the whole unbinding process. To verify this hypothesis, at least for a representative melatonin receptor ligand, we investigated the reasons for the stereoselectivity of UCM1014 enantiomers. The tetrahydroquinoline derivative UCM1014 is a potent MT_2-selective agonist previously characterized as a racemic mixture. The stereoselectivity observed for the desmethoxy analog (62-fold higher binding affinity of the (−)- than the (+)-enantiomer) led us to predict the (*R*)-enantiomer of UCM1014 as the eutomer on the basis of a ligand-based pharmacophore hypothesis.[19] The enantiomers of UCM1014 were synthesized separately with known stereochemistry, confirming the (*R*)-enantiomer as the more potent. Investigation of the binding mode of (*R*)- and (*S*)-UCM1014 allowed to ascribe the different potency to a conformational selection operated by the receptor. The (*R*)-enantiomer was docked in the binding site with axial arrangement of the amide side chain, that is, in the most abundant conformation in solution, as experimentally observed for the desmethoxy analog.[19] On the contrary, the (*S*)-enantiomer could interact with $Gln194^{ECL2}$ only in the less populated conformation having equatorial side chain. Additionally, metadynamics simulations of the MT_1 or MT_2 receptor-(*R*)-UCM1014 complex confirmed that the axial arrangement is the preferred one also inside the receptor and that the equatorial side chain can contribute to receptor binding as well. The simulations performed on UCM1014 prove that molecular models based on already established ligand-receptor interactions can effectively explain non-trivial structural aspects (i.e., stereoselectivity) and binding affinities measured in standard conditions (2 h of incubation time) which, even if not obtained in equilibrium conditions, effectively approximate values observed at longer times.

AUTHOR CONTRIBUTIONS

Annalida Bedini: Analysis and interpretation of data, writing. **Gian Marco Elisi**: Molecular modeling. **Fabiola Fanini**: Synthesis and compound characterization. **Michele Retini**: Synthesis and compound characterization. **Laura Scalvini**: Molecular modeling. **Silvia Rivara**: Conception and design, analysis and interpretation of data, writing. **Chiara Contri**: Binding experiments. **Katia Varani**: Conception and design, supervision. **Gilberto Spadoni**: Conception and design, supervision. **Marco Mor**: Conception and design, supervision. **Fabrizio Vincenzi**: Conception and design, analysis and interpretation of data, writing. **Silvia Pasquini**: Binding experiments. All authors revised the manuscript and approved the submitted version.

ACKNOWLEDGMENTS

This research benefitted from the High-Performance Computing facility of the University of Parma, Italy (http://www.hpc.unipr.it) and the support of CINECA through ISCRA C projects (*es_MT$_{1\text{-}2}$*, id HP10CB3GC3, and *MT$_1$-kin*, id HP10CI4MQB, to G. M. E). CHO cells expressing the MT_1 and MT_2 receptors are a kind gift of Dr. Jean Boutin (Les Laboratoires Servier). This work was supported by the Italian Ministry for University and Research (MIUR, PRIN 2017, 20175SA5JJ project), by funding obtained under the National Recovery and Resilience Plan (NRRP), Mission 4 Component 2 Investment 1.3—Call for tender No. 341 of 15/03/2022 of the Italian Ministry of University and Research funded by the European Union—NextGenerationEU, Project code PE0000006, Concession Decree No. 1553 of 11/10/2022 adopted by the Italian Ministry of University and Research, CUP D93C22000930002, "A multiscale integrated approach to the study of the nervous system in health and disease" (MNESYS), and by funding co-financed by the European Union "FSE-REACT-EU, PON Research and innovation 2014-2020 DM 1062/2021" (CUP H31B21009610007—research contract: 63-G-19602-1).

CONFLICT OF INTEREST STATEMENT

The authors declare no conflict of interest.

DATA AVAILABILITY STATEMENT

Data that support the findings of this study are available in the Supporting Information section and from the corresponding author upon request.

ORCID

Annalida Bedini https://orcid.org/0000-0002-9103-2918
Gian Marco Elisi https://orcid.org/0000-0001-9071-5621
Fabiola Fanini https://orcid.org/0000-0002-8392-2881
Michele Retini https://orcid.org/0000-0003-0218-8505

Laura Scalvini https://orcid.org/0000-0003-3610-527X
Silvia Pasquini https://orcid.org/0000-0001-9442-1428
Chiara Contri https://orcid.org/0000-0003-3936-5923
Katia Varani https://orcid.org/0000-0003-4562-1348
Gilberto Spadoni https://orcid.org/0000-0001-7253-6902
Marco Mor https://orcid.org/0000-0003-0199-1849
Fabrizio Vincenzi https://orcid.org/0000-0002-5027-1699
Silvia Rivara https://orcid.org/0000-0001-8058-4250

REFERENCES

1. Dubocovich ML, Takahashi JS. Use of 2-[^{125}I]iodomelatonin to characterize melatonin binding sites in chicken retina. *Proc Natl Acad Sci USA*. 1987;84:3916-3920.
2. Gbahou F, Jockers R. 2-[^{125}I]Iodomelatonin and [^{3}H]melatonin binding assays for melatonin receptors. *Methods Mol Biol*. 2022;2550:141-149.
3. Vakkuri O, Lämsä E, Rahkamaa E, Ruotsalainen H, Leppäluoto J. Iodinated melatonin: preparation and characterization of the molecular structure by mass and ^{1}H NMR spectroscopy. *Anal Biochem*. 1984;142:284-289.
4. Glatfelter GC, Jones AJ, Rajnarayanan RV, Dubocovich ML. Pharmacological actions of carbamate insecticides at mammalian melatonin receptors. *J Pharmacol Exp Ther*. 2021;376:306-321.
5. Rivara S, Lodola A, Mor M, et al. *N*-(substituted-anilinoethyl) amides: design, synthesis, and pharmacological characterization of a new class of melatonin receptor ligands. *J Med Chem*. 2007;50:6618-6626.
6. Ferreira Jr., MA, Azevedo H, Mascarello A, et al. Discovery of ACH-000143: a novel potent and peripherally preferred melatonin receptor agonist that reduces liver triglycerides and steatosis in diet-induced obese rats. *J Med Chem*. 2021;64:1904-1929.
7. Audinot V, Mailliet F, Lahaye-Brasseur C, et al. New selective ligands of human cloned melatonin MT_1 and MT_2 receptors. *Naunyn Schmiedebergs Arch Pharmacol*. 2003;367:553-561.
8. Nishiyama K, Hirai K. In vitro comparison of duration of action of melatonin agonists on melatonin MT_1 receptor: possible link between duration of action and dissociation rate from receptor. *Eur J Pharmacol*. 2015;757:42-52.
9. Legros C, Devavry S, Caignard S, et al. Melatonin MT_1 and MT_2 receptors display different molecular pharmacologies only in the G-protein coupled state. *Br J Pharmacol*. 2014;171:186-201.
10. Guo D, Hillger JM, IJzerman AP, Heitman LH. Drug-target residence time—a case for G protein-coupled receptors. *Med Res Rev*. 2014;34:856-892.
11. Disse B, Reichl R, Speck G, Traunecker W, Rominger KL, Hammer R. Ba 679 BR, a novel long-acting anticholinergic bronchodilator. *Life Sci*. 1993;52:537-544.
12. Disse B, Speck GA, Rominger KL, Witek TJ, Hammer R. Tiotropium (Spiriva): mechanistical considerations and clinical profile in obstructive lung disease. *Life Sci*. 1999;64:457-464.
13. Pan AC, Borhani DW, Dror RO, Shaw DE. Molecular determinants of drug–receptor binding kinetics. *Drug Discov Today*. 2013;18:667-673.
14. Sohraby F, Nunes-Alves A. Advances in computational methods for ligand binding kinetics. *Trends Biochem Sci*. 2023;48(5):437-449.
15. Bernetti M, Masetti M, Rocchia W, Cavalli A. Kinetics of drug binding and residence time. *Annu Rev Phys Chem*. 2019;70:143-171.
16. Stauch B, Johansson LC, McCorvy JD, et al. Structural basis of ligand recognition at the human MT_1 melatonin receptor. *Nature*. 2019;569:284-288.
17. Sugden D, Pickering H, Teh MT, Garratt PJ. Melatonin receptor pharmacology: toward subtype specificity. *Biol Cell*. 1997;89:531-537.
18. Dubocovich ML, Masana MI, Iacob S, Sauri DM. Melatonin receptor antagonists that differentiate between the human Mel1a and Mel1b recombinant subtypes are used to assess the pharmacological profile of the rabbit retina ML1 presynaptic heteroreceptor. *Naunyn Schmiedebergs Arch Pharmacol*. 1997;355:365-375.
19. Spadoni G, Bedini A, Lucarini S, et al. Highly potent and selective MT_2 melatonin receptor full agonists from conformational analysis of 1-benzyl-2-acylaminomethyl-tetrahydroquinolines. *J Med Chem*. 2015;58:7512-7525.
20. Johansson LC, Stauch B, McCorvy JD, et al. XFEL structures of the human MT_2 melatonin receptor reveal the basis of subtype selectivity. *Nature*. 2019;569:289-292.
21. Abraham MJ, Murtola T, Schulz R, et al. GROMACS: high performance molecular simulations through multi-level parallelism from laptops to supercomputers. *SoftwareX*. 2015;1-2:19-25.
22. Tribello GA, Bonomi M, Branduardi D, Camilloni C, Bussi G. PLUMED2: new feathers for an old bird. *Comput Phys Commun*. 2014;185:604-613.
23. Essmann U, Perera L, Berkowitz ML, Darden T, Lee H, Pedersen LG. A smooth particle mesh Ewald method. *J Chem Phys*. 1995;103:8577-8593.
24. Hess B, Bekker H, Berendsen HJC, Fraaije JGEM. LINCS: a linear constraint solver for molecular simulations. *J Comput Chem*. 1997;18:1463-1472.
25. Nosé S. A molecular dynamics method for simulations in the canonical ensemble. *Mol Phys*. 1984;52:255-268.
26. Hoover WG. Canonical dynamics: equilibrium phase-space distributions. *Phys Rev A*. 1985;31:1695-1697.
27. Kästner J. Umbrella sampling. *Wiley Interdiscip. Rev. Comput. Mol. Sci*. 2011;1:932-942.
28. Kumar S, Rosenberg JM, Bouzida D, Swendsen RH, Kollman PA. The weighted histogram analysis method for free energy calculations on biomolecules. I. The method. *J Comput Chem*. 1992;13:1011-1021.
29. Barducci A, Bussi G, Parrinello M. Well-tempered metadynamics: a smoothly converging and tunable free-energy method. *Phys Rev Lett*. 2008;100:020603.
30. Bussi G, Laio A. Using metadynamics to explore complex free-energy landscapes. *Nat Rev Phys*. 2020;2:200-212.
31. Scalvini L, Vacondio F, Bassi M, et al. Free-energy studies reveal a possible mechanism for oxidation-dependent inhibition of MGL. *Sci Rep*. 2016;6:31046.
32. Hulme EC, Trevethick MA. Ligand binding assays at equilibrium: validation and interpretation. *Br J Pharmacol*. 2010;161:1219-1237.

33. Cheng Y, Prusoff WH. Relationship between the inhibition constant (K_i) and the concentration of inhibitor which causes 50% inhibition (I_{50}) of an enzymatic reaction. *Biochem Pharmacol*. 1973;22:3099-3108.
34. Kenakin T. The measurement of receptor signaling bias. *Methods Mol Biol*. 2015;1335:163-176.
35. Dupré C, Bruno O, Bonnaud A, et al. Assessments of cellular melatonin receptor signaling pathways: β-arrestin recruitment, receptor internalization, and impedance variations. *Eur J Pharmacol*. 2018;818:534-544.
36. Li A, Liu S, Huang R, Ahn S, Lefkowitz RJ. Loss of biased signaling at a G protein-coupled receptor in overexpressed systems. *PLoS ONE*. 2023;18:e0283477.
37. Cecon E, Oishi A, Jockers R. Melatonin receptors: molecular pharmacology and signalling in the context of system bias. *Br J Pharmacol*. 2018;175:3263-3280.
38. Elisi GM, Scalvini L, Lodola A, Mor M, Rivara S. Free-energy simulations support a lipophilic binding route for melatonin receptors. *J Chem Inf Model*. 2022;62:210-222.
39. Mazna P, Grycova L, Balik A, et al. The role of proline residues in the structure and function of human MT_2 melatonin receptor. *J Pineal Res*. 2008;45:361-372.
40. Ballesteros JA, Weinstein H. Integrated methods for the construction of three-dimensional models and computational probing of structure-function relations in G protein-coupled receptors. *Methods Neurosci*. 1995;25:366-428.
41. Boutin JA, Witt-Enderby PA, Sotriffer C, Zlotos DP. Melatonin receptor ligands: a pharmaco-chemical perspective. *J Pineal Res*. 2020;69:e12672.
42. Zlotos DP, Jockers R, Cecon E, Rivara S, Witt-Enderby PA. MT_1 and MT_2 melatonin receptors: ligands, models, oligomers, and therapeutic potential. *J Med Chem*. 2014;57:3161-3185.
43. Legros C, Matthey U, Grelak T, et al. New radioligands for describing the molecular pharmacology of MT_1 and MT_2 melatonin receptors. *Int J Mol Sci*. 2013;14:8948-8962.
44. Legros C, Brasseur C, Delagrange P, Ducrot P, Nosjean O, Boutin JA. Alternative radioligands for investigating the molecular pharmacology of melatonin receptors. *J Pharmacol Exp Ther*. 2016;356:681-692.
45. Jarmoskaite I, AlSadhan I, Vaidyanathan PP, Herschlag D. How to measure and evaluate binding affinities. *eLife*. 2020;9:e57264.
46. Szlenk CT, Gc JB, Natesan S. Does the lipid bilayer orchestrate access and binding of ligands to transmembrane orthosteric/allosteric sites of G protein-coupled receptors? *Mol Pharmacol*. 2019;96:527-541.
47. Payandeh J, Volgraf M. Ligand binding at the protein-lipid interface: strategic considerations for drug design. *Nat Rev Drug Discov*. 2021;20:710-722.
48. Lane JR, Sexton PM, Christopoulos A. Bridging the gap: bitopic ligands of G-protein-coupled receptors. *Trends Pharmacol Sci*. 2013;34(1):59-66.
49. Elisi GM, Scalvini L, Lodola A, Bedini A, Spadoni G, Rivara S. *In silico* drug discovery of melatonin receptor ligands with therapeutic potential. *Expert Opin Drug Discov*. 2022;17:343-354.
50. Spadoni G, Bedini A, Furiassi L, et al. Identification of bivalent ligands with melatonin receptor agonist and fatty acid amide hydrolase (FAAH) inhibitory activity that exhibit ocular hypotensive effect in the rabbit. *J Med Chem*. 2018;61:7902-7916.
51. Cammarota M, Ferlenghi F, Vacondio F, et al. Combined targeting of fatty acid amide hydrolase and melatonin receptors promotes neuroprotection and stimulates inflammation resolution in rats. *Br J Pharmacol*. 2023;180:1316-1338.

SUPPORTING INFORMATION

Additional supporting information can be found online in the Supporting Information section at the end of this article.

How to cite this article: Bedini A, Elisi GM, Fanini F, et al. Binding and unbinding of potent melatonin receptor ligands: mechanistic simulations and experimental evidence. *J Pineal Res*. 2024;76:e12941. doi:10.1111/jpi.12941